Inorg. Chem. **2002**, *41*, 1404–1411

Two New Terpyridine Dimanganese Complexes: A Manganese(III,III) Complex with a Single Unsupported Oxo Bridge and a Manganese(III,IV) Complex with a Dioxo Bridge. Synthesis, Structure, and Redox Properties

Carole Baffert,[1a] Marie-Noëlle Collomb,*[,1a,b] Alain Deronzier,[1a] Jacques Pécaut,[1c] Julian Limburg,[1b] Robert H. Crabtree,[1b] and Gary W. Brudvig[1b]

Laboratoire d'Electrochimie Organique et de Photochimie Rédox, CNRS UMR 5630, Université Joseph Fourier, BP 53, 38041 Grenoble Cedex 9, France, Department of Chemistry, Yale University, P.O. Box 208107, New Haven, Connecticut 068520-8107, and DRFMC—Laboratoire de Chimie Inorganique et Biologique, UMR CEA-CNRS-UJF 5046, CEA-Grenoble, 38054 Grenoble Cedex, France

Received July 11, 2001

Two new terpyridine dimanganese oxo complexes $[Mn_2^{III,IV}(\mu\text{-}O)_2(terpy)_2(CF_3CO_2)_2]^+$ (**3**) and $[Mn_2^{III,III}(\mu\text{-}O)(terpy)_2(CF_3CO_2)_4]$ (**4**) (terpy = 2,2′:6,2″-terpyridine) have been synthesized and their X-ray structures determined. In contrast to the corresponding mixed-valent aqua complex $[Mn_2^{III,IV}(\mu\text{-}O)_2(terpy)_2(H_2O)_2]^{3+}$ (**1**), the two Mn atoms in **3** are not crystallographically equivalent. The neutral binuclear monooxo manganese(III,III) complex **4** exhibits two crystallographic forms having cis and trans configurations. In the cis complex, the two $CF_3CO_2^-$ ligands on each manganese adopt a cis geometry to each other; one $CF_3CO_2^-$ is trans to the oxygen of the oxo bridge while the second is cis. In the trans complex, the two coordinated $CF_3CO_2^-$ have a trans geometry to each other and are cis to the oxo bridge. The electrochemical behavior of **3** in organic medium (CH_3CN) shows that this complex could be oxidized into its corresponding stable manganese(IV,IV) species while its reduced form manganese(III,III) is very unstable and leads by a disproportionation process to Mn(II) and Mn(IV) complexes. Complex **4** is only stable in the solid state, and it disproportionates spontaneously in CH_3CN solution into the mixed-valent complex **3** and the mononuclear complex $[Mn^{II}(terpy)_2]^{2+}$ (**2**), thereby preventing the observation of its electrochemical behavior.

Introduction

The oxygen-evolving complex (OEC) of photosystem II (PSII) consists of a μ-oxo-bridged manganese tetramer associated with Ca^{2+}, Cl^-, and a redox-active tyrosine that can carry out the four-electron oxidation of water to dioxygen.[2] Very recently, the first X-ray structure of PSII to 3.8 Å resolution was reported from the thermophilic cyanobacterium *Synechococcus elongatus*.[3] This structure provides new information on the position, size, and shape of the manganese cluster. However, the distance between the metal ions, their identity, and how the bonds are constructed cannot be deduced at this stage. Up to now, structural and manganese valence information has mainly been obtained by EXAFS and EPR spectroscopy. These studies have established the presence of two di-μ-oxo bridged pairs of manganese linked by a system of oxo and carboxylato bridges.[4] This assignment was made by comparison with the large number of structural model complexes with various ligands.[5] In contrast, few studies concerning the reactivities of such molecular models toward water oxidation have been published.[6]

* To whom correspondence should be addressed. E-mail: Marie-Noelle.Collomb@ujf-grenoble.fr. Fax: 33 4 76 51 42 67.

(1) (a) Laboratoire d'Electrochimie Organique et de Photochimie Rédox, Université Joseph Fourier. (b) Department of Chemistry, Yale University. (c) Laboratoire de Chimie Inorganique et Biologique.

(2) (a) Debus, R. J. *Biochim. Biophys. Acta* **1992**, *1102*, 269. (b) Britt, R. D. In *Oxygenic Photosynthesis: The Light Reactions*; Ort, D. R., Yocum, C. F., Eds.; Advances in Photosynthesis, Vol. 4; Kluwer Academic Publishers: Dordrecht, The Netherlands, 1996; pp 137–159. (c) Vrettos, J. S.; Limburg, J.; Brudvig, G. W. *Biochim. Biophys. Acta* **2001**, *1503*, 229. (d) Rüttinger, W.; Dismukes, G. C. *Chem. Rev.* **1997**, *97*, 1.

(3) Zouni, A.; Witt, H.-T.; Kern, J.; Fromme, P.; Krauss, N.; Saenger, W.; Orth, P. *Nature* **2001**, *409*, 739.

(4) (a) Yachandra, V. K.; DeRose, V. J.; Latimer, M. J.; Mukerjee, I.; Sauer, K.; Klein, M. P. *Science* **1993**, *260*, 675. (b) Yachandra, V. K.; Sauer, K.; Klein, M. P. *Chem. Rev.* **1996**, *96* , 2927.

10.1021/ic0107375 CCC: $22.00
Published on Web 02/20/2002

Recently, some of the authors of this article reported a reaction of sodium hypochlorite (NaOCl) with the complex $[Mn_2^{III,IV}(\mu\text{-}O)_2(terpy)_2(H_2O)_2]^{3+}$ (**1**) (terpy = 2,2′:6,2″-terpyridine) as a catalyst, that resulted in the catalytic formation of O_2, but **1** was deactivated by the irreversible formation of permanganate.[7] This was the first report of a di-μ-oxo complex, a structural model for the manganese complex in the OEC, that could carry out catalytic O−O bond formation. Complementary to the use of OCl^-, these authors have also studied the O_2-evolving reaction with another oxidant (oxone, $KHSO_5$) with Mn(II) and Mn(III) mononuclear $[Mn(L)_2]^n$ complexes containing the planar tridentate ligands terpyridine ($n = +2$, complex **2**) and dipicolinate ($n = -1$) respectively, where mixed-valence di-μ-oxo dimers formed in situ.[8] Complex **1** can also catalyze water oxidation when HSO_5^- is used as a primary oxidant.[9] The proposed mechanism involves formation of O_2 by reaction of a formally Mn(V)═O intermediate with outer sphere water/hydroxide or oxone.

In this context, knowledge of the redox properties of **1** and **2** would be helpful for an understanding of the reaction mechanisms involved in these functional models. In this article, we focus on the electrochemical properties of dimanganese terpyridine complexes in organic solution (CH_3CN); measurements in aqueous medium will be described elsewhere.[10]

Because **1** is insoluble in CH_3CN, we report here the synthesis of the analogous dimanganese(III,IV) complexes in which the aqua ligands are substituted by $CF_3CO_2^-$ anions, $[Mn_2^{III,IV}(\mu\text{-}O)_2(terpy)_2(CF_3CO_2)_2](X)$ (X = $CF_3CO_2^-$ (**3a**) and ClO_4^- (**3b**)), which are soluble in CH_3CN. Complex **3b** was structurally characterized. Furthermore, during attempts to crystallize complex **3a**, we have isolated a novel dimanganese(III,III) complex $[Mn_2^{III,III}(\mu\text{-}O)(terpy)_2(CF_3CO_2)_4]$ (**4**) which possesses an unsupported monooxo bridge with a linear Mn(III)−O−Mn(III) unit and two coordinated $CF_3CO_2^-$ on each manganese. Dinuclear complexes in which Mn atoms are bridged by a single oxo group are still rare.[11] We report here the structural characterization of this complex. Two types of crystals were obtained. In one case, the two $CF_3CO_2^-$ ligands on each manganese adopt a cis geometry to each other (*cis*-**4**), while in the second type they are *trans* (*trans*-**4**).

Experimental Section

Materials. Tetra-*n*-butylammonium perchlorate (Bu_4NClO_4), tetraethylammonium trifluoroacetate ($Et_4NCF_3CO_2$), and sodium trifluoroacetate ($NaCF_3CO_2$) were purchased from Fluka. Acetonitrile (CH_3CN, Rathburn, HPLC grade) was used as received and stored under an argon atmosphere in a glovebox. The ligand 2,2′:6′,2″-terpyridine (terpy) was purchased from Aldrich.

Synthesis of Complexes. $[Mn_2^{III,IV}(\mu\text{-}O)_2(terpy)_2(H_2O)_2](NO_3)_3\cdot 6H_2O$ (Complex 1). This complex was obtained according to methods described previously.[7,12]

$[Mn^{II}(terpy)_2](BF_4)_2$ (Complex 2). A solution of 0.21 g of $Mn(O_2CCH_3)_2\cdot 4H_2O$ (0.86 mmol) in 7 mL of H_2O was added to 0.40 g of terpy (1.71 mmol) in 8 mL of acetone. The resulting yellow solution was stirred for 15 min and filtered. A H_2O solution of 0.3 g (2.72 mmol) of sodium tetrafluoroborate was then added to the solution which was cooled to 0 °C. After 3 days, the yellow precipitate that formed was filtered and then redissolved in CH_3CN. The solution was filtered to remove some impurities. Addition of diethyl ether induced the precipitation of the complex as a yellow powder (0.54 g, yield 91%). IR in cm^{-1} (KBr): $\nu = 3399$ (s), 3066 (w), 1600 (s), 1579 (m), 1563 (w), 1479 (s), 1453 (s), 1437 (m), 1318 (m), 1249 (m), 1190 (w), 1162 (m), 1107 (s), 1060 (vs), 1021 (s), 770 (vs), 651 (m), 639 (w), 521 (w), 425 (w), 403 (w). Symbols: br, broad; vs, very strong; s, strong; m, medium; w, weak; sh, shoulder. Electronic spectral data in CH_3CN solution (λ_{max} in nm (ϵ in $M^{-1}\ cm^{-1}$)): 230 (37300), 265 (17800), 275 (19500), 284 (23100), 323 (30600), 335 (30500).

$[Mn_2^{III,IV}(\mu\text{-}O)_2(terpy)_2(CF_3CO_2)_2](CF_3CO_2)\cdot 2H_2O$ (Complex 3a·2H2O). This complex was obtained according to a method similar to that described previously for the synthesis of **1**,[7] except that $NaCF_3CO_2$ was used to precipitate the complex instead of KNO_3. $Mn(CH_3CO_2)_2\cdot 4H_2O$ (0.105 g, 0.428 mmol) and terpy (0.100 g, 0.428 mmol) were dissolved in 3 mL of H_2O. A solution of oxone ($2KHSO_5\cdot KHSO_4\cdot K_2SO_4$) (0.111 g, 0.189 mmol) in 2 mL of H_2O was added dropwise with stirring, causing the yellow solution to turn dark green. After stirring at room temperature for 10 min, the solution was cooled to 0 °C. The addition of a large excess of solid $NaCF_3CO_2$ (3 g, 22 mmol) precipitated the complex **3a**·$2H_2O$ as a dark-green pure microcrystalline product, as shown by elemental analysis (0.163 g, yield 82%). This product analyzed satisfactorily as $[Mn_2^{III,IV}(\mu\text{-}O)_2(terpy)_2(CF_3CO_2)_2](CF_3CO_2)\cdot 2H_2O$. Elemental anal. Calcd for complex **3a** ($C_{36}H_{26}Mn_2N_6O_{10}F_9$ (983.5)): C, 43.97; H, 2.66; N, 8.54. Found: C, 43.91; H, 2.43; N, 8.54. IR in cm^{-1} (KBr): $\nu = 3448$ (s), 3077 (w), 2924 (w), 1688 (vs), 1599 (m), 1575 (w), 1562 (w), 1500 (w), 1478 (m), 1451 (m), 1430 (w), 1418 (w), 1326 (w), 1313 (w), 1248 (w), 1203 (vs), 1172 (sh), 1124 (s), 1053 (w), 1046 (w), 1025 (w), 1014 (w), 838 (w), 827 (w), 797 (m), 778 (m), 720 (m), 706 (w), 674 (w), 668 (w), 651 (w), 640 (w), 601 (w), 516 (w), 454 (w), 439 (w), 410 (w). Electronic spectral data in CH_3CN solution (λ_{max} in nm (ϵ in $M^{-1}\ cm^{-1}$)): 278 (31000), 324 (25000), 550 (725), 620 (650). Single crystals of complex **3** were only obtained as a ClO_4^- salt (complex **3b**).

$[Mn_2^{III,IV}(\mu\text{-}O)_2(terpy)_2(CF_3CO_2)_2](ClO_4)\cdot CH_3CN$ (Complex 3b·CH3CN). Five milliliters of a saturated CH_3CN solution of Bu_4NClO_4 was added to a green solution of complex **3a**·$2H_2O$ (0.136

(5) See for instance: (a) Manchanda, R.; Brudvig, G. W.; Crabtree, R. H. *Coord. Chem. Rev.* **1995**, *144*, 1. (b) Wieghardt, K *Angew. Chem., Int. Ed. Engl.* **1994**, *33*, 725.
(6) Yagi, M.; Kaneko, M. *Chem. Rev.* **2001**, *101*, 21.
(7) Limburg, J.; Vrettos, J. S.; Liable-Sands, L. M.; Rheingold, A. L.; Crabtree, R. H.; Brudvig, G. W. *Science* **1999**, *283*, 524.
(8) (a) Limburg, J.; Brudvig, G. W.; Crabtree, R. H. *J. Am. Chem. Soc.* **1997**, *119*, 2761. (b) Limburg, J.; Crabtree, R. H.; Brudvig, G. W. *Inorg. Chim. Acta* **2000**, *297*, 301.
(9) Limburg, J.; Vrettos, J. S.; Chen, H.; De Paula, J. C.; Crabtree, R. H.; Brudvig, G. W. *J. Am. Chem. Soc.* **2001**, *123*, 423.
(10) Richardot, A.; Baffert, C.; Collomb, M.-N.; Deronzier, A. Manuscript in preparation.
(11) (a) Ziolo, R. F.; Stanford, R. H.; Rossman, G. R.; Gray, H. B. *J. Am. Chem. Soc.* **1974**, *96*, 7910. (b) Kipke, C. A.; Scott, M. J.; Gohdes, J. W.; Armstrong, W. H. *Inorg. Chem.* **1990**, *29*, 2193. (c) Kitajima, N.; Osawa, M.; Tanaka, M.; Moro-oka, Y. *J. Am. Chem. Soc.* **1991**, *113*, 8952. (d) Horwitz, C. P.; Ciringh, Y. *Inorg. Chim. Acta* **1994**, *225*, 191. (e) Horner, O.; Anxolabéhère-Mallart, E.; Charlot, M.-F.; Tchertanov, L.; Guilhem, J.; Mattioli, T. A.; Boussac, A.; Girerd, J.-J. *Inorg. Chem.* **1999**, *38*, 1222.
(12) Collomb, M.-N.; Deronzier, A.; Richardot, A.; Pécaut, J. *New J. Chem.* **1999**, *23*, 351.

g, 0.145 mmol) in 15 mL of CH_3CN. The green precipitate obtained was collected by filtration, washed thoroughly with CH_2Cl_2, and dried under air (0.104 g, yield 78%).

CAUTION! Perchlorate salts of compounds containing organic ligands are potentially explosive. Although we have encountered no such problems with complex 3b, only small quantities of these compounds should be prepared and handled with care.

Single crystals of $[Mn_2^{III,IV}(\mu\text{-}O)_2(terpy)_2(CF_3CO_2)_2](ClO_4)\cdot CH_3CN$ were grown by slow diffusion of ethyl acetate into a concentrated solution of **3b** in CH_3CN (yield 90%). These crystals analyzed satisfactorily as $[Mn_2^{III,IV}(\mu\text{-}O)_2(terpy)_2(CF_3CO_2)_2](ClO_4)\cdot CH_3CN$. Elemental anal. Calcd for complex **3a** ($C_{36}H_{25}Mn_2N_7O_{10}F_6Cl_1$ (974.96)): C, 44.35; H, 2.58; N, 10.06. Found: C, 44.55; H, 2.69; N, 10.14. IR in cm^{-1} (KBr): ν = 3429 (s), 3079 (w), 2921 (w), 1698 (vs), 1651 (w), 1644 (w), 1600 (m), 1574 (w), 1538 (w), 1504 (w), 1478 (m), 1450 (m), 1417 (m), 1326 (w), 1313 (w), 1246 (w), 1198 (vs), 1138 (s), 1090 (vs), 1044 (w), 1025 (w), 1015 (w), 841 (w), 792 (w), 777 (s), 722 (m), 706 (m), 675 (w), 658 (w), 650 (w), 639 (w), 624 (w), 606 (w), 515 (w), 452 (w), 415 (w). This complex exhibits the same UV−visible spectrum in CH_3CN solution as that of **3a**·$2H_2O$.

$[Mn_2^{III,III}(\mu\text{-}O)(terpy)_2(CF_3CO_2)_4]$ (Complex 4). Single crystals of this complex were obtained by attempts to crystallize complex **3a**. Indeed, slow diffusion of CH_2Cl_2 into a concentrated solution of **3a** in CH_3CN afforded green-turquoise crystals of **4** suitable for X-ray diffraction analysis (yield 30%). X-ray analysis of two different samples have shown two types of crystals. Single crystals of *cis*-CF_3CO_2 $[Mn_2^{III,III}(\mu\text{-}O)(terpy)_2(CF_3CO_2)_4]\cdot H_2O\cdot 2CH_2Cl_2$ (*cis*-**4**·H_2O·$2CH_2Cl_2$) and *trans*-CF_3CO_2 $[Mn_2^{III,III}(\mu\text{-}O)(terpy)_2(CF_3CO_2)_4]\cdot {}^3/_2CH_2Cl_2$ (*trans*-**4**·$^3/_2CH_2Cl_2$) were obtained. Upon standing in air (few minutes), crystals of the cis and trans complexes are transformed into a green-turquoise powder due to loss of CH_2Cl_2. All measurements in solution, especially electrochemistry, were made with this amorphous material. This material analyzed satisfactorily as $[Mn_2^{III,III}(\mu\text{-}O)(terpy)_2(CF_3CO_2)_4]$. Elemental anal. Calcd for complex **4** ($C_{38}H_{22}Mn_2N_6O_9F_{12}$ (1044.49)): C, 43.70; H, 2.12; N, 8.05. Found: C, 44.05; H, 2.32; N, 8.35. IR in cm^{-1} (KBr): ν = 3429 (s), 3077 (w), 2920 (w), 1682 (vs), 1605 (m), 1575 (w), 1557 (w), 1538 (w), 1505 (w), 1480 (m), 1454 (m), 1410 (m), 1318 (w), 1195 (vs), 1131 (s), 1026 (w), 879 (m), 835 (w), 795 (w), 774 (m), 720 (m), 652 (w), 640 (w), 518 (w), 417 (w), 367 (w), 333 (w).

X-ray Structure Analysis. The data sets for the single-crystal X-ray studies were collected with Mo Kα radiation on a Brucker SMART diffractometer. All calculations were performed on a Silicon Graphics system using the SHELXTL program.[13] The specific data for the crystals and the refinements are collected in Tables 1 and 2. The structures were solved by direct methods and refined by full-matrix least-squares fits of F_2.

Electrochemistry. Electrochemical measurements were carried out using an EG&G PAR model 173 potenstiostat equipped with a model 179 digital coulometer and a model 175 programmer with output recorded on a Sefram TGM 164 $X-Y$ recorder. Cyclic voltammetric studies (E_{pa}, anodic peak potential; E_{pc}, cathodic peak potential; $E_{1/2} = (E_{pa} + E_{pc})/2$; $\Delta E_p = E_{pa} - E_{pc}$) and exhaustive electrolyses were run under an argon atmosphere in a glovebox at room temperature, using a standard three-electrode electrochemical cell. The electrolyte was a 0.1 M solution of Bu_4NClO_4 or 0.1 M $Et_4NCF_3CO_2$, in CH_3CN. All potentials were referred to an Ag/Ag^+ (10 mM) reference electrode in CH_3CN, 0.1 M Bu_4NClO_4. The potential of the regular ferrocene/ferrocenium (Fc/Fc^+) redox couple used as an internal standard was $E_{1/2}$ = 0.07 V under our experimental conditions. Working electrodes were platinum disks polished with 1 μm diamond paste, that were 5 mm in diameter for cyclic voltammetry (CV) and 2 mm in diameter for rotating disk electrode experiments (RDE). Exhaustive electrolyses were carried out with a 5 cm^2 platinum cylinder or a 10 × 10 × 4 mm^3 carbon felt electrode (RCV 2000, 65 mg cm^{-3}, from Le Carbone Lorraine).

Spectroscopies. Electronic absorption spectra were recorded on a Cary 1 Varian spectrophotometer or on a Hewlett-Packard 8452A diode array spectrophotometer. Initial and electrolyzed solutions were transferred to a conventional cuvette cell in the glovebox. The cell was inserted into an optical translator connected to the spectrophotometer through a fiber optic system (Photonetics Spectrofip System). The optical fibers pass through the wall of the drybox via seals. EPR spectra were recorded at 100 K on a Bruker ESP 300E spectrometer operating at 9.4 GHz (X band). Infrared

Table 1. Crystallographic Data and Parameters for $[Mn_2^{III,IV}(\mu\text{-}O)_2(terpy)_2(CF_3CO_2)_2](ClO_4)\cdot CH_3CN$ (**3b**·CH_3CN)

chem formula	$C_{36}H_{25}ClF_6Mn_2N_7O_{10}$
fw	974.96
temp/K	193(2)
λ (Å)	0.71073
cryst syst	monoclinic
cryst size (mm × mm × mm)	0.2 × 0.2 × 0.5
space group	$P2(1)/n$
a (Å)	9.6174(6)
b (Å)	22.0264(13)
c (Å)	18.1985(11)
α (deg)	90
β (deg)	100.8680(10)
γ (deg)	90
V (Å^3)	3786(4)
Z	4
δ_{calcd} (g cm^{-3})	1.710
F (000)	1964
abs coeff, mm^{-1}	0.837
no. of reflns collcd	24176
no. of indep reflns	9057 [R_{int} = 0.0325]
GOF on F^2	0.937
final R indices [$I > 2\sigma(I)$]	R1 = 0.0370, wR2 = 0.0946
R indices (all data)	R1 = 0.0686, wR2 = 0.1102
largest diff peak, hole (e Å^{-3})	0.956, −0.883

Table 2. Crystallographic Data and Parameters for *cis*-**4**·H_2O·$2CH_2Cl_2$ and *trans*-**4**·$^3/_2CH_2Cl_2$

compound	*cis*-**4**·H_2O·$2CH_2Cl_2$	*trans*-**4**·$^3/_2CH_2Cl_2$
chemical formula	$C_{40}H_{28}Cl_4F_{12}Mn_2N_6O_{10}$	$C_{39.5}H_{25}Cl_3F_{12}Mn_2N_6O_9$
fw	1232.36	1171.89
temp/K	193(2)	293(2)
λ (Å)	0.71073	0.71073
cryst syst	monoclinic	triclinic
cryst size (mm × mm × mm)	0.2 × 0.2 × 0.4	0.04 × 0.4 × 0.5
space group	$C2/c$	$P\bar{1}$
a (Å)	18.528(2)	14.447(4)
b (Å)	16.6292(16)	15.875(5)
c (Å)	16.9803(17)	20.926(6)
α (deg)	90	93.488(5)
β (deg)	117.838(2)	94.889(5)
γ (deg)	90	101.781(6)
V (Å^3)	4626.2(8)	4666(2)
Z	4	4
δ_{calcd} (g cm^{-3})	1.769	1.668
abs coeff (mm^{-1})	0.890	0.821
F (000)	2464	2340
no. of reflns collcd	9003	29083
no. of indep reflns	5198 [R_{int} = 0.0507]	21215 [R_{int} = 0.0394]
GOF on F^2	1.262	1.092
final R indices [$I > 2\sigma(I)$]	R1 = 0.0869, wR2 = 0.2302	R1 = 0.0706, wR2 = 0.1827
R indices (all data)	R1 = 0.1735, wR2 = 0.2519	R1 = 0.1298, wR2 = 0.2068
largest diff peak, hole (e Å^{-3})	1.219, −1.328	1.471, −0.968

(13) Sheldrick, G. M. *SHELXTL*, version 5.1; Siemens Analytical X-Ray Instruments: Madison, WI, 1990.

spectra were recorded with a Perkin-Elmer Spectrum GX FTIR spectrometer as KBr pellets.

Results and Discussion

Syntheses. As for many other dimanganese(III,IV) di-μ-oxo bridged complexes,[7,12,14] the di-μ-oxo terpyridine complexes are obtained from the corresponding mononuclear Mn(II) precursor by oxidation with 1.5 equiv of a chemical oxidizing agent. $[Mn_2^{III,IV}(\mu\text{-}O)_2(terpy)_2(H_2O)_2]^{3+}$ (**1**) is synthesized first by HSO_5^- oxidation of the in situ generated $[Mn^{II}(terpy)_2]^{2+}$ complex (**2**) in an aqueous solution. $[Mn_2^{III,IV}(\mu\text{-}O)_2(terpy)_2(CF_3CO_2)_2](CF_3CO_2)\cdot 2H_2O$ (**3a**$\cdot 2H_2O$) is then obtained as a green microcrystalline powder by addition of an excess of $NaCF_3CO_2$ to the solution containing **1**. Despite many attemps, we were unable to obtain single crystals of this complex due to the competitive crystallization of the neutral compound $[Mn_2^{III,III}(\mu\text{-}O)(terpy)_2(CF_3CO_2)_4]$ (**4**). Crystals of complex **3** were obtained by displacement of the counteranion $CF_3CO_2^-$ by ClO_4^- (see Experimental Section). Single crystals of the complex $[Mn_2^{III,IV}(\mu\text{-}O)_2(terpy)_2(CF_3CO_2)_2](ClO_4)\cdot CH_3CN$ (**3b**$\cdot CH_3CN$) were then grown with a good yield (90%) by slow diffusion of ethyl acetate into a CH_3CN solution of this complex. Complexes **3a**$\cdot 2H_2O$ and **3b**$\cdot CH_3CN$ exhibit IR spectra similar to that of complex **1**, with the di-oxo-bridge band located at 706 cm^{-1}. Additional bands characteristic of the trifluoroacetate absorptions are also observed at 1688, 1203, 1124, 838, 797, and 720 cm^{-1}. For complex **3b**$\cdot CH_3CN$, the absorptions of perchlorate are observed at 1090 and 624 cm^{-1}. Complexes **3a**$\cdot 2H_2O$ and **3b**$\cdot CH_3CN$ are soluble and stable in CH_3CN, giving dark green solutions.

On the other hand, single crystals of complex **4** were obtained by slow diffusion of CH_2Cl_2 into a concentrated solution of complex **3a**$\cdot 2H_2O$ in CH_3CN. During the crystallization, besides the crystals of complex **4**, a brown precipitate of MnO_2 is also formed. This result shows that **4** is probably formed by a disproportionation reaction (eq 1),

$$2[Mn_2^{III,IV}(\mu\text{-}O)_2(terpy)_2(CF_3CO_2)_2](CF_3CO_2) + H_2O \rightarrow [Mn_2^{III,III}(\mu\text{-}O)(terpy)_2(CF_3CO_2)_4] + 2(Mn^{IV}O_2)_x + 2CF_3CO_2^- + 2terpy + 2H^+ \quad (1)$$

where $(Mn^{IV}O_2)_x$ denotes that the manganese dioxide is aggregated. The poor yield of **4** (30%), with respect to the total manganese, supports the hypothesis of a disproportionative process. X-ray analysis of several samples of crystals has shown that **4** can crystallize in two different forms: $[Mn_2^{III,III}(\mu\text{-}O)(terpy)_2(CF_3CO_2)_4]\cdot H_2O\cdot 2CH_2Cl_2$ (*cis*-**4**$\cdot H_2O\cdot 2CH_2Cl_2$) and $[Mn_2^{III,III}(\mu\text{-}O)(terpy)_2(CF_3CO_2)_4]\cdot {}^3/_2CH_2Cl_2$ (*trans*-**4**$\cdot 3/2CH_2Cl_2$). In *cis*-**4**$\cdot H_2O\cdot 2CH_2Cl_2$, the two $CF_3CO_2^-$ ligands on each manganese adopt a cis geometry to each other, while in complex *trans*-**4**$\cdot 3/2CH_2Cl_2$, they are trans. Complexes **4** are neutral; therefore, the valence of both manganese ions is ascribed to Mn(III). The typical band of the di-μ-oxo bridge located at 706 cm^{-1} is absent in the IR spectra of these complexes,[11] while the $CF_3CO_2^-$ bands are located at 1682, 1195, 1131, 835, 795, and 720 cm^{-1}. Complexes **4** are insoluble in pure CH_3CN or in CH_3CN containing 0.1 M $Et_4CF_3CO_2$; however, after few a minutes, they disproportionate in these solvents to give a mixture of the soluble mononuclear and binuclear complexes **2** and **3**, respectively (see Electrochemistry section).

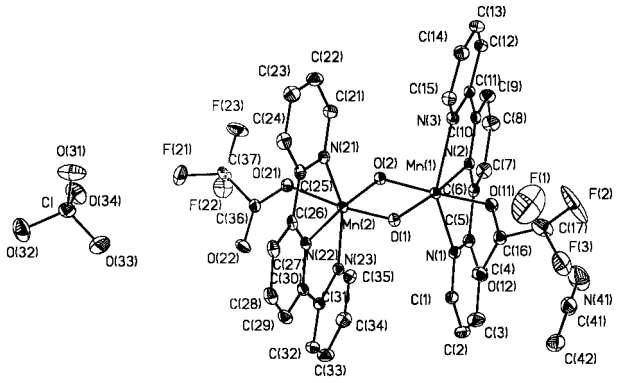

Figure 1. An ORTEP view of $[Mn_2^{III,IV}(\mu\text{-}O)_2(terpy)_2(CF_3CO_2)_2](ClO_4)\cdot CH_3CN$, complex **3b**$\cdot CH_3CN$.

Description of the Crystal Structures. Complex 3b·CH_3CN. The ORTEP diagram of the cation $[Mn_2^{III,IV}(\mu\text{-}O)_2(terpy)_2(CF_3CO_2)_2]^+$ is represented in Figure 1. The geometry at each manganese is approximately octahedral, with the coordination spheres consisting of the three N atoms from a single terpy ligand, the two μ-oxo ligands, and the O atom of the coordinated trifluoroacetate. The geometry is similar to those observed in **1**[7,12] and the recently crystallographically characterized $[Mn_2^{IV,IV}(\mu\text{-}O)_2(terpy)_2(SO_4)_2]$ dimer.[9] The Mn−Mn bond distance of 2.7265 (5) Å in **3b** compares well with that observed in **1** (2.7315(12) Å) and is at the high end of the range (2.588−2.741 Å) observed for other structurally characterized $Mn^{III}Mn^{IV}$ di-oxo-bridged complexes.[15] In contrast to **1**, where Mn(III) and Mn(IV) are crystallographically equivalent,[7,12] the bond lengths to the two Mn atoms in complex **3b** clearly indicate that they are of different valence. The smaller distances about Mn(2) compared to Mn(1) indicate that this atom is Mn(IV), a d^3 ion. Furthermore, the geometry of Mn(1) is typical of a d^4 high-spin Mn(III) ion because of the elongation of the bonds to the two pyridyl N atoms coordinated in the axial positions (Jahn−Teller distortion). The Mn(1)−N_{ax} distances are 0.13 Å longer than the Mn(1)−N_{eq} distance, while these distances are within the range for a normal d^3 ion for Mn(2) (Mn(2)−N_{ax} are 0.02 Å longer than Mn(2)−N_{eq}) (Table 3). Moreover, the EPR spectrum of this complex in CH_3CN shows the characteristic 16-line pattern, indicating a d-electron-localized species.

The Mn(1)−O distances (average 1.8512 Å) and Mn(2)−O distances (average 1.7741 Å) for the oxo bridges are consistent with the values observed in the $[Mn_2^{III,IV}(\mu\text{-}O)_2(L)_4]^{3+}$ complexes (L = 2,2′-bipyridine (bpy) (average 1.854 and 1.784 Å)[16] and 1,10-phenanthroline (phen) (average

(14) (a) Cooper, S. R.; Calvin, M. *J. Am. Chem. Soc*. **1977**, *99*, 6623. (b) Manchanda, R.; Brudvig, G. W.; De Gala, S.; Crabtree, R. H. *Inorg. Chem.* **1994**, *33*, 5157.

(15) Pal, S.; Olmstead, M. M.; Armstrong, W. H. *Inorg. Chem*. **1995**, *34*, 4708 and references therein.

Table 3. Selected Bond Lengths (Å) and Bond Angles (deg) for **3b**·CH_3CN

Mn(1)−Mn(2)	2.7265(5)		
Mn(1)−$O(1)_{oxo}$	1.8517(16)	Mn(2)−$O(1)_{oxo}$	1.7786(17)
Mn(1)−$O(2)_{oxo}$	1.8508(17)	Mn(2)−$O(2)_{oxo}$	1.7696(16)
Mn(1)−$O(11)_{eq}$	1.9914(18)	Mn(2)−$O(21)_{eq}$	2.0104(17)
Mn(1)−$N(1)_{ax}$	2.255(2)	Mn(2)−$N(21)_{ax}$	2.031(2)
Mn(1)−$N(2)_{eq}$	2.1284(19)	Mn(2)−$N(22)_{eq}$	2.0051(19)
Mn(1)−$N(3)_{ax}$	2.272(2)	Mn(2)−$N(23)_{ax}$	2.021(2)
Mn(1)−O(1)−Mn(2)	97.46(7)	Mn(1)−O(2)−Mn(2)	97.69(8)
O(1)−Mn(1)−O(2)	80.28	O(1)−Mn(2)−O(2)	84.10(7)
O(1)−Mn(1)−O(11)	95.05(7)	O(2)−Mn(2)−O(21)	90.78(7)
O(2)−Mn(1)−O(11)	172.36(8)	O(1)−Mn(2)−O(21)	173.46(7)
O(1)−Mn(1)−N(1)	102.77(7)	O(2)−Mn(2)−N(21)	90.78(7)
O(1)−Mn(1)−N(2)	166.11(7)	O(2)−Mn(2)−N(22)	174.10(8)
O(1)−Mn(1)−N(3)	112.90(7)	O(2)−Mn(2)−N(23)	99.31(8)
N(1)−Mn(1)−N(2)	73.44(7)	N(21)−Mn(2)−N(22)	78.19(8)
N(2)−Mn(1)−N(3)	73.06(7)	N(22)−Mn(2)−N(23)	78.75(8)
N(1)−Mn(1)−N(3)	143.92(7)	N(21)−Mn(2)−N(23)	155.58(8)

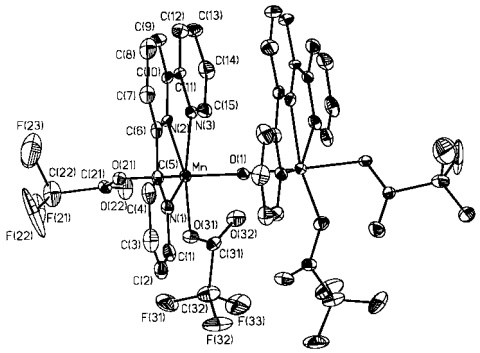

A

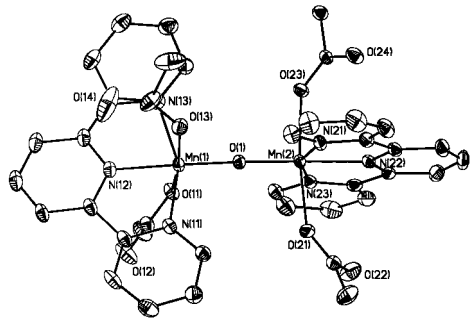

B

Figure 2. ORTEP views of $[Mn_2^{III,III}(\mu\text{-O})(terpy)_2(CF_3CO_2)_4]$, complex **4**: (A) *cis*-**4**·H_2O·$2CH_2Cl_2$ and (B) *trans*-**4**·$^3/_2CH_2Cl_2$ (fluoro atoms are omitted for clarity).

1.848 and 1.775 Å)).[14b] The Mn−O bond lengths of 1.9914(18) and 2.0104(17) Å for the trifluoroacetate ligands compare well with those observed in $[Fe_2^{III,III}(\mu\text{-O})(dmbpy)_4(CF_3CO_2)_2]^{2+}$ (dmbpy = 4,4′-dimethyl-2,2′-bipyridine) (1.985(6) and 1.995(6) Å).[17] The octahedral coordination polyhedra are highly distorted, with cis angles ranging from 73.06(7)° to 112.90(7)° for Mn(1) and 78.19(8)° to 104.41(8)° for Mn(2) for angles that would be 90° in a perfect octahedron.

Complexes *cis*-4·H_2O·$2CH_2Cl_2$ and *trans*-4·$^3/_2CH_2Cl_2$. Figure 2 shows the ORTEP diagrams of the two crystallographic forms of the neutral binuclear complex $[Mn_2^{III,III}(\mu\text{-O})(terpy)_2(CF_3CO_2)_4]$: *cis*-**4**·$H_2O$·$2CH_2Cl_2$ (Figure 2A) and *trans*-**4**·$^3/_2CH_2Cl_2$ (Figure 2B). Table 2 contains crystallographic data, and Tables 4 and 5 contain selected bond distances and angles. The two manganese are equivalent in *cis*-**4**·H_2O·$2CH_2Cl_2$ because the halves of the dimer are related by a 2-fold axis which runs through the bridging oxygen atom. In the case of the crystals of *trans*-**4**·$^3/_2CH_2Cl_2$, the unit cell contains four binuclear complexes, two of which are distinct but very similar; therefore, only one is shown Figure 2B and discussed below. In the cis and trans complexes, the Mn(III) centers are approximately octahedrally coordinated with each Mn atom bound by the three N atoms from one terpy ligand, the O atoms of the two coordinated $CF_3CO_2^-$, and the bridging oxide. In the cis complex, the two coordinated $CF_3CO_2^-$ on each manganese adopt a cis geometry to each other; one $CF_3CO_2^-$ is trans to the O of the oxo bridge while the second is cis (Figure 2A). The two planes defined by the terpy ligands in the cis complex are almost parallel to each other, as in other crystallographically characterized di-μ-oxo terpy complexes **1**, **3**, and $[Mn_2^{IV,IV}(O)_2(terpy)_2(SO_4)_2]$.[7,9,12] The geometry of the trans complex is very different. The two coordinated $CF_3CO_2^-$ on each manganese adopt a trans geometry to each other and are cis to the oxo bridge. Moreover, the two terpy ligands are perpendicular to each other (Figure 2B). The Mn−O bond lengths of 2.163, 2.174, 2.178, and 2.175 Å for the $CF_3CO_2^-$ ligands in the trans complex are significantly longer than those of 1.967 and 1.974 Å in the cis complex and than values observed for **3b**·CH_3CN (Table 3). This can be explained by different axes for the Jahn−Teller distortion. There is an elongation of the bonds to the trans $CF_3CO_2^-$ ligands in the trans complex while the axial elongation involves the terminal pyridine groups of the terpy ligand in the cis complex. The Mn−O_{oxo} distance of 1.7471(10) Å in the cis complex is consistent with the values of 1.754 and 1.751 Å observed in the trans complex and is comparable to the Mn−O_{oxo} distances in the other structurally characterized complexes containing the Mn(III)−O−Mn(III)

Table 4. Selected Bond Lengths (Å) and Bond Angles (deg) for *cis*-**4**·H_2O·$2CH_2Cl_2$

Mn−Mn#	3.493	Mn−N(1)	2.235(5)
Mn−$O(1)_{oxo}$	1.7471(10)	Mn−N(2)	2.160(6)
Mn−O(21)	1.967(4)	Mn−N(3)	2.221(5)
Mn−O(31)	1.974(5)		
Mn−O(1)−Mn#	176.7(4)	O(1)−Mn−N(3)	92.32(17)
O(1)−Mn−O(21)	178.14(18)	N(1)−Mn−N(2)	73.0(2)
O(1)−Mn−O(31)	94.3(2)	N(2)−Mn−N(3)	73.6(2)
O(1)−Mn−N(1)	89.85(14)	N(1)−Mn−N(3)	146.6(2)
O(1)−Mn−N(2)	92.5(2)		

Table 5. Selected Bond Lengths (Å) and Bond Angles (deg) for *trans*-**4**·$^3/_2CH_2Cl_2$

Mn(1)−Mn(2)	3.504		
Mn(1)−$O(1)_{oxo}$	1.751(3)	Mn(2)−$O(1)_{oxo}$	1.754(3)
Mn(1)−O(11)	2.178(3)	Mn(2)−O(21)	2.163(3)
Mn(1)−O(13)	2.175(3)	Mn(2)−$O(23)_{eq}$	2.174(3)
Mn(1)−N(11)	2.087(4)	Mn(2)−$N(21)_{ax}$	2.090(4)
Mn(1)−N(12)	1.993(4)	Mn(2)−$N(22)_{eq}$	1.990(4)
Mn(1)−N(13)	2.108(4)	Mn(2)−$N(23)_{ax}$	2.104(4)
Mn(1)−$O(1)_{oxo}$−Mn(2)	178.00(18)		
O(1)−Mn(1)−O(11)	92.21(13)	O(1)−Mn(2)−O(21)	101.04(4)
O(1)−Mn(1)−O(13)	103.00(14)	O(1)−Mn(2)−O(23)	102.90(14)
O(1)−Mn(1)−N(11)	101.44(14)	O(1)−Mn(2)−N(21)	93.35(13)
O(1)−Mn(1)−N(12)	176.75(14)	O(1)−Mn(2)−N(22)	178.77(14)
O(1)−Mn(1)−N(13)	91.82(13)	O(1)−Mn(2)−N(23)	93.42(12)
N(11)−Mn(1)−N(12)	78.18(15)	N(21)−Mn(2)−N(22)	78.43(15)
N(12)−Mn(1)−N(13)	77.58(16)	N(22)−Mn(2)−N(23)	77.61(15)
N(11)−Mn(1)−N(13)	155.38(15)	N(21)−Mn(2)−N(23)	155.99(14)

(16) Plaksin, P. M.; Stoufer, R. C.; Mathew, M.; Palenik, G. J. *J. Am. Chem. Soc.* **1972**, *94*, 2121.
(17) Ménage, S.; Vincent, J.-M.; Lambeaux, C.; Chottard, G.; Grand, A.; Fontecave, M. *Inorg. Chem.* **1993**, *32*, 4766.

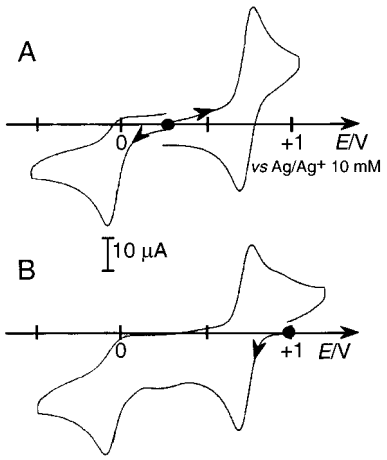

Figure 3. Cyclic voltammograms at a platinum electrode in CH_3CN, 0.1 M Bu_4ClO_4, sweep rate $v = 100$ mV s^{-1}: (A) of a 0.64 mM solution of **3**; (B) after exhaustive oxidation of the solution in part A at 1 V.

core (1.72−1.77 Å).[11a−c,e] The Mn−O−Mn bridges are almost linear (176.7° and 178° in the cis and trans complexes, respectively), and the Mn−Mn distances (3.493 and 3.504 Å) are consistent with a Mn(III)−O−Mn(III) core structure.[11b,c,e] The mean intraligand angle for N−Mn−N of terpy in the cis form (average value 73.3°) is about 5° smaller than that in the trans form (average value 77.95°), reflecting the axial elongation of the pyridyl bonds in the cis complex.

Electrochemistry. Electrochemical Behavior of 3. The CV of **3** in CH_3CN, 0.1 M Bu_4ClO_4 (Figure 3A) exhibits one reversible oxidation wave at $E_{1/2} = +0.74$ V vs Ag/Ag^+ (10 mM) ($\Delta E_p = 60$ mV) and an irreversible reduction at $E_{pc} = -0.08$ V corresponding to the Mn_2(III,IV)/Mn_2(IV,IV) and Mn_2(III,IV)/Mn_2(III,III) redox couples, respectively (eqs 2 and 3).

$$[Mn_2^{III,IV}(\mu\text{-}O)_2(terpy)_2(CF_3CO_2)_2]^+ \underset{b}{\overset{a}{\rightleftarrows}} [Mn_2^{IV,IV}(\mu\text{-}O)_2(terpy)_2(CF_3CO_2)_2]^{2+} + e^- \quad (2)$$

$$[Mn_2^{III,IV}(\mu\text{-}O)_2(terpy)_2(CF_3CO_2)_2]^+ + e^- \rightarrow [Mn_2^{III,III}(\mu\text{-}O)_2(terpy)_2(CF_3CO_2)_2] \quad (3)$$

Controlled potential coulometry establishes that each wave is a one-electron process. An exhaustive oxidation at 1 V of the solution consumes one electron per molecule of **3**. The oxidized species $[Mn_2^{IV,IV}(\mu\text{-}O)_2(terpy)_2(CF_3CO_2)_2]^{2+}$ is obtained with a 95% yield as attested by the relative height of the waves at a rotating disk electrode. The CV of the resulting solution exhibits the typical electroactivity of this Mn_2(IV,IV) species with its reversible reduction at +0.74 V and the irreversible peak at −0.08 V (Figure 3B) from the reduction of the Mn_2(III,IV) complex.

Figure 4 illustrates the UV−visible spectra before and after electrolysis at +1 V. The spectrum of the initial green solution of **3** is close to that of **1** in H_2O[12] and shows two visible bands at 620 and 550 nm and two UV bands at 324 and 278 nm. The fully oxidized brown solution of the (IV,IV) species exhibits three visible bands at 664, 554, and 408 nm and two UV bands at 314 (shoulder at 336) and 280

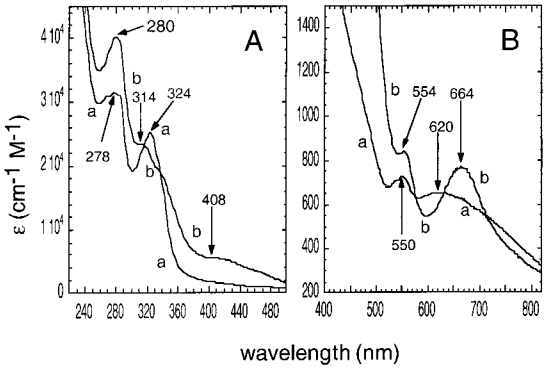

Figure 4. Changes in the UV−visible absorption spectra of a 0.64 mM solution of **3** in CH_3CN, 0.1 M Bu_4ClO_4: (a) initial solution; (b) after exhaustive oxidation at 1 V.

nm. As expected, a subsequent controlled-potential reduction at +0.45 V of the oxidized solution consumes 0.95 electron per molecule of initial complex **3** and restores 95% of the initial amount of **3** (eq 2b).

On the other hand, a controlled-potential reduction at −0.30 V of a solution of **3** (1 mM) in CH_3CN, 0.1 M Bu_4ClO_4 consumes also one electron per binuclear complex. The electrochemical and spectroscopic characteristics of the reduced solution are identical to those of a chemical sample of the mononuclear complex **2** in the same medium. The CV of **2** shows, as observed previously,[18] a quasi-reversible oxidation wave at $E_{1/2} = 1.01$ V vs Ag/Ag^+ (10 mM), while the absorption spectrum shows the five UV−visible bands of this complex at 230, 265, 275, 284, 323, and 335 nm. The amount of **2** is estimated to 1 mM using the ϵ values of these bands from a chemical sample of **2**. A brown side product which is partially soluble is also formed in solution during the electrolysis and probably corresponds to manganese oxide, as observed during the electroreduction of the $[Mn_2^{III,IV}(\mu\text{-}O)_2(bpy)_4]^{3+}$ complex[19] in CH_3CN. Equation 4 summarizes the proposed overall process. An exhaustive

$$[Mn_2^{III,IV}(\mu\text{-}O)_2(terpy)_2(CF_3CO_2)_2]^+ + e^- \underset{b}{\overset{a}{\rightleftarrows}} [Mn^{II}(terpy)_2]^{2+} + (Mn^{IV}O_2)_x + 2CF_3CO_2^- \quad (4)$$

reoxidation of this solution at 1.0 V followed by a reduction at 0.65 V restores almost entirely the initial amount of the binuclear μ-oxo−dimanganese(III,IV) complex (eq 4b). It should be noted that the brown precipitate is entirely redissolved during the oxidation process. This demonstrates that the overall process (eq 4) is chemically reversible. In summary it appears that the new di-μ-oxo $Mn_2^{III,IV}$ complex, **3**, exhibits a behavior similar to that of other μ-oxo complexes, such as $[Mn_2O_2(bpy)_4]^{3+}$ or $[Mn_2O_2(phen)_4]^{3+}$.[20] However, **3** is significantly easier to oxidize ($E_{1/2} = 0.74$ V) and more difficult to reduce ($E_{pc} = -0.08$ V) compared to the bpy and phen complexes ($E_{1/2} = 1.01$ and 0.05 V;[20c,d] $E_{pc} = 1.00$ and 0.06 V,[20e] respectively). This is a consequence of the negative charge and greater donor property of the $CF_3CO_2^-$ ligand.

(18) Morrison, M. M.; Sawyer, D. T. *Inorg. Chem.* **1978**, *17*, 333.
(19) Collomb Dunand-Sauthier, M.-N.; Deronzier, A. *J. Electroanal. Chem.* **1997**, *428*, 65.

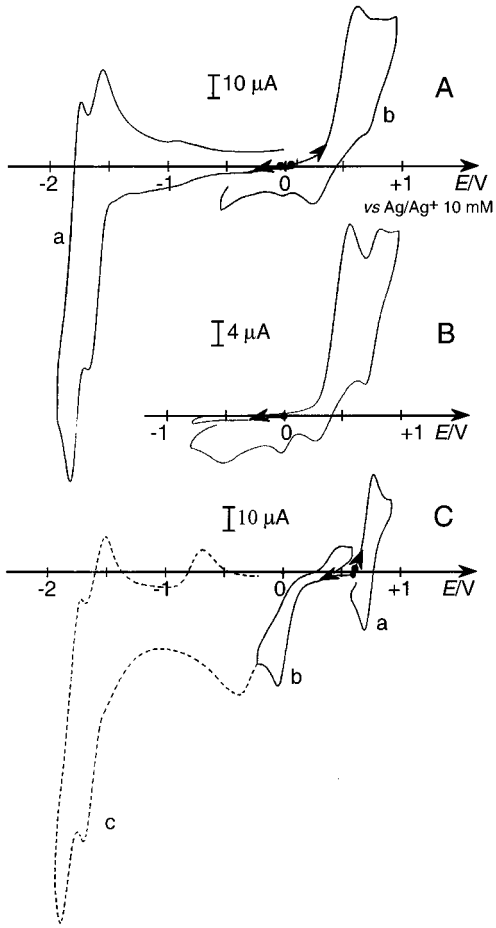

Figure 5. Cyclic voltammograms at a platinum electrode in CH_3CN, 0.1 M $Et_4CF_3CO_2$ of a 2 mM solution of **2**, sweep rate $\upsilon = 100$ mV s^{-1} (A); $\upsilon = 20$ mV s^{-1} (B); after exhaustive oxidation of the solution in part A at 0.6 V, sweep rate $\upsilon = 100$ mV s^{-1} (C).

Electrochemical Properties of 2 in CH_3CN, 0.1 M $Et_4NCF_3CO_2$. A previous study by Morrison and Sawyer[18] has shown that electrochemical oxidation of $[Mn^{II}(L)_3]^{2+}$ complexes (L = bpy and phen, substituted or not) in CH_3CN, 0.1 M Bu_4NClO_4 leads to formation of the corresponding $[Mn_2^{III,IV}(\mu\text{-}O)_2(L)_4]^{3+}$ binuclear complexes. In contrast, they also reported that electrochemical oxidation of **2** in the same electrolyte does not yield a clean dimerization reaction, but rather leads to the formation of unidentified species. We find that a clean dimerization reaction occurs upon electrochemical oxidation of **2**, leading to the formation of **3**, if $Et_4NCF_3CO_2$ is used as supporting electrolyte instead of Bu_4NClO_4. The formation of **3** is due to the presence of the coordinating $CF_3CO_2^-$ anions.

The negative region of the CV of **2** in CH_3CN with 0.1 M $Et_4NCF_3CO_2$ shows two reversible waves at $E_{1/2} = -1.61$ V ($\Delta E_p = 80$ mV) and $E_{1/2} = -1.78$ V ($\Delta E_p = 60$ mV) vs Ag/Ag^+ (10 mM) corresponding to the successive one-electron ligand-centered reductions of **2** (Figure 5A and eq 5). This behavior is the same as in 0.1 M Bu_4NClO_4.

$$[Mn^{II}(terpy)_2]^{2+} \underset{-e^-}{\overset{+e^-}{\rightleftharpoons}} [Mn^{II}(terpy)$$

$$E_{1/2} = -1.61 \text{ V}$$

$$(terpy^{\bullet-})^+ \underset{-e^-}{\overset{+e^-}{\rightleftharpoons}} [Mn^{II}(terpy^{\bullet-})_2] \quad (5)$$

$$E_{1/2} = -1.78 \text{ V}$$

In the positive region, the CV of **2** exhibits an irreversible oxidation peak at $E_{pa} = 0.60$ V corresponding to a metal-centered oxidation process (Figure 5A,B). The irreversibility of this peak is due to the formation of **3** as evidenced by the presence of its reversible oxidation wave at $E_{1/2} = 0.74$ V, which follows the irreversible oxidation peak of **2**, and irreversible reduction peak at $E_{pc} = -0.08$ V on the reverse scan. It should be noted that **2** is more easily oxidized with $Et_4NCF_3CO_2$ as supporting electrolyte than with Bu_4NClO_4 ($E_{1/2} = 1.01$ V). This difference is probably due to the coordination of $CF_3CO_2^-$ to Mn in the chemical reactions that follow the electron transfer.

Traces A and B in Figure 5 display the CVs of **2** recorded at different potential scan rates. The relative intensities of the oxidation and reduction waves of the binuclear complex **3** compared to that of the irreversible oxidation peak of **2** increase when the scan rate decreases. It is apparent that, at a slow scan rate ($\upsilon = 20$ mV s^{-1}), formation of **3** is more effective.

A controlled-potential oxidation of a 1 mM solution of **2** at 0.6 V consumes 1.3 electrons per mole of **2** and furnishes a green solution that exhibits the spectroscopic and electrochemical characteristics of a solution of **3** (Figure 5C). The amount of **3** is estimated to be 0.48 mM (yield 96%) by its visible absorption band at $\lambda_{max} = 620$ nm using the ϵ value of 650 M^{-1} cm^{-1} (see Experimental Section). The reaction mechanism involved in the formation of **3** is probably similar to those observed for the formation of the bpy and phen di-μ-oxo binuclear complexes in CH_3CN from electrochemical oxidations of the corresponding mononuclear Mn(II) complexes.[18] The reaction follows from the instability of the one-electron-oxidized form of **2**, $[Mn^{III}(terpy)_2]^{3+}$, which leads to the Mn_2(III,IV) complex via release of one terpy ligand, interaction with residual water in CH_3CN, and Mn disproportionation, as shown in eq 6a.

$$2[Mn^{II}(terpy)_2]^{2+} + 2H_2O + 2CF_3CO_2^- \underset{b}{\overset{a}{\rightleftharpoons}} [Mn_2^{III,IV}(\mu\text{-}O)_2$$
$$(terpy)_2(CF_3CO_2)_2]^+ + 2terpyH_2^{2+} + 3e^- \quad (6)$$

We have confirmed the release of one terpy ligand and two protons upon oxidation of **2** by CV analysis of the oxidized solution conducted between 0.0 and -2.3 V (Figure 5C). The irreversible peak at -0.38 V is typical of the reduction of $terpyH_2^{2+}$ at a Pt electrode. Moreover, this reduction peak is shifted to -0.56 V at a vitreous carbon electrode. It should be noted that the transformation of **2** into **3** is a reversible process, as attested by the observation of the two typical reversible redox waves of **2** in the CV, at potentials lower than that for the reduction of free $terpyH_2^{2+}$.

(20) (a) Morrison, M. M.; Sawyer, D. T. *J. Am. Chem. Soc.* **1977**, *99*, 257. (b) Cooper, S. R.; Calvin, M. *J. Am. Chem. Soc.* **1977**, *99*, 6623. (c) Collomb Dunand-Sauthier, M.-N.; Deronzier, A.; Pradon, X.; Menage, S.; Philouze, C. *J. Am. Chem. Soc.* **1997**, *119*, 3173. (d) Collomb Dunand-Sauthier, M.-N.; Deronzier, A.; Piron, A.; Pradon, X.; Menage, S. *J. Am. Chem. Soc.* **1998**, *120*, 5373. (e) Collomb Dunand-Sauthier, M.-N.; Deronzier, A. *J. Electroanal. Chem.* **1997**, *463*, 119.

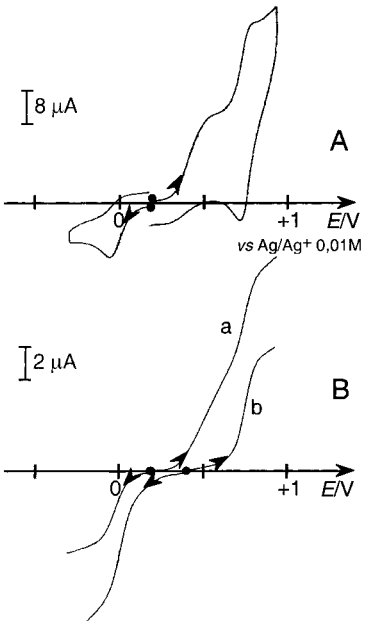

Figure 6. Voltammograms at a platinum electrode in CH_3CN, 0.1 M Et_4-CF_3CO_2, sweep rate $v = 100$ mV s^{-1}: (A) of a 0.7 mM solution of **4**; (B) at a platinum rotating disk electrode, scan rate $v = 10$ mV s^{-1}, $\omega = 600$ rotations min^{-1}, curve a, of a 0.7 mM solution of **4**; curve b, after exhaustive oxidation of the solution in part a at 0.65 V.

This is confirmed by a controlled-potential reduction at −0.15 V which consumes 1.5 electrons per binuclear complex and regenerates a solution of **2** with a 94% yield (eq 6b). On the other hand, as expected, the $[Mn_2^{IV,IV}(\mu\text{-O})_2(terpy)_2(CF_3CO_2)_2]^{2+}$ complex can be generated from the oxidation at 0.95 V of the solution of **3**. This subsequent oxidation consumes an additional 0.6 electron per molecule of initial **2** and gives the Mn_2(IV,IV) species with a 95% yield.

Electrochemical Behavior of 4. The dissolution of **4** (0.85 mM) in CH_3CN (see Experimental Section) results in its disproportionation into **2** and **3** within a few minutes (eq 7).

$$2[Mn_2^{III,III}(\mu\text{-O})(terpy)_2(CF_3CO_2)_4] \underset{b}{\overset{a}{\rightleftharpoons}} [Mn_2^{III,IV}(\mu\text{-O})_2(terpy)_2(CF_3CO_2)_2]^+ + [Mn^{II}(terpy)_2]^{2+} + Mn^{3+} + 6CF_3CO_2^- \quad (7)$$

This reaction is clearly shown in the CV of the resulting solution after addition of 0.1 M $Et_4NCF_3CO_2$ as supporting electrolyte (Figure 6) which exhibits the typical electrochemical oxidations of both complexes. The concentration of each complex has been estimated to about 0.4 mM by the height of the two corresponding waves at a Pt rotating disk electrode (compared to the height of pure chemical samples of these complexes) (Figure 6B). A controlled-potential oxidation of the solution at 0.65 V, which consumes about 1.2 electrons per molecule of initial **4**, furnishes a green solution containing only **3**. Equation 8 summarizes the overall process.

$$[Mn_2^{III,IV}(\mu\text{-O})_2(terpy)_2(CF_3CO_2)_2]^+ + [Mn^{II}(terpy)_2]^{2+} + Mn^{3+} + 6CF_3CO_2^- + H_2O \rightarrow 2[Mn_2^{III,IV}(\mu\text{-O})_2(terpy)_2(CF_3CO_2)_2]^+ + 4CF_3CO_2H + 2e^- \quad (8)$$

Conclusion

We have prepared several new oxo dimanganese terpy complexes that are soluble in organic solvents. This has enabled characterization of the electrochemical properties of the di-μ-oxo dimanganese complex **3** in CH_3CN. A new stable Mn(IV,IV) complex can be formed by a one-electron reversible oxidation of complex **3**.

In contrast, the corresponding III,III complex is very unstable and leads by a disproportionation process to Mn(II) and Mn(IV) complexes. However, the overall transformations are fully reversible.

These studies provide information on the redox properties of di-μ-oxo dimanganese complexes related to complex **1**. Complex **1** catalyzes O_2 evolution in aqueous solution, and the O−O bond-forming step was proposed to involve a formally Mn(V)═O intermediate. However, a Mn(V) intermediate was not observed in the present study; only the Mn_2(IV,IV) oxidation state can be reached by electrochemical oxidation of **3** in CH_3CN. The presence of the $CF_3CO_2^-$ ligands may prevent the formation of a possible Mn(V)═O species.

The study of the electrochemical properties of **1** in aqueous solution will provide key insights into the reaction mechanisms involved during the catalytic O_2 evolution. Two type of results can be expected. The first is generation of oxidation states higher than IV with the formation of one or more terminal oxo ligands, as proposed in the case of water oxidation catalysis by **1** in the presence of chemical oxidants and observed for $[Ru_2^{III,III}(\mu\text{-O})(bpy)_4(H_2O)_2]^{4+}$.[21] Another possibility is the formation of oxo bridges between the one-electron-oxidized species $[Mn_2^{IV,IV}(\mu\text{-O})_2(terpy)_2(H_2O)_2]^{4+}$ giving tetranuclear or polymeric complexes. Indeed, we have clearly shown from electrochemical studies of $[Mn_2^{III,IV}(\mu\text{-O})_2(L)_4]^{3+}$ complexes (L = bpy, phen) in aqueous solution the significant tendency of the Mn(IV) species to aggregate and to form the tetranuclear complexes $[Mn_4^{IV}(\mu\text{-O})_6(L)_6]^{6+}$.[20c−e] It should be noted that, in the case of the terpy complexes, this transformation is possible with no loss of terpy ligand. Preliminary results for **1** in aqueous solution indicate that aggregate formation does occur. Further characterization of this process is currently underway.

Acknowledgment. We thank Dr. Carole Duboc-Toia for her assistance on EPR experiments. M.-N.C. would like to thank NATO and the Centre National de la Recherche Scientifique for financial support. The National Institutes of Health (Grant GM32715) funded the work done at Yale University.

Supporting Information Available: Crystallographic details for complexes **3b**, *cis*-**4**, and *trans*-**4** in CIF format. This material is available free of charge via the Internet at http://pubs.acs.org.

IC0107375

(21) Gersten, S. W.; Samuels, G. S.; Meyer, T. J. *J. Am. Chem. Soc.* **1985**, *107*, 3853.